



HAL
open science

Generalizations of the gyroid surface

A. Fogden, M. Haeberlein, S. Lidin

► **To cite this version:**

A. Fogden, M. Haeberlein, S. Lidin. Generalizations of the gyroid surface. Journal de Physique I, 1993, 3 (12), pp.2371-2385. 10.1051/jp1:1993250 . jpa-00246873

HAL Id: jpa-00246873

<https://hal.science/jpa-00246873>

Submitted on 4 Feb 2008

HAL is a multi-disciplinary open access archive for the deposit and dissemination of scientific research documents, whether they are published or not. The documents may come from teaching and research institutions in France or abroad, or from public or private research centers.

L'archive ouverte pluridisciplinaire **HAL**, est destinée au dépôt et à la diffusion de documents scientifiques de niveau recherche, publiés ou non, émanant des établissements d'enseignement et de recherche français ou étrangers, des laboratoires publics ou privés.

Classification
Physics Abstracts
02.40 — 68.00

Generalizations of the gyroid surface

A. Fogden, M. Haerberlein (*) and S. Lidin

Inorganic Chemistry 2, Chemical Centre, PO Box 124, S-22100 Lund, Sweden

(Received 19 March 1993, accepted in final form 19 August 1993)

Abstract. — The deformation of Schoen's gyroid — one of the three examples of triply-periodic minimal surfaces possessing cubic symmetry and genus 3 — is discussed. Lower-symmetry variants (similarly of genus 3) are shown to exist, and the one-variable family of rhombohedrally-distorted gyroids is constructed and parametrised exactly *via* the Weierstrass representation.

Introduction.

We regard structure as the manifestation of the coupling of our two basic concepts of force and geometry. Our scientific understanding relies upon the construction of model systems facilitating a decoupling of the two concepts. By means of this decomposition we establish separate sets of rules governing each. These rules then permit assessment of the level of interplay between the two in a particular structure — the first step towards solution of the problem as a whole. One may argue that, with increasing sophistication of computer simulation techniques, a detailed knowledge of force laws alone may suffice, circumventing this first step. However geometry will remain the ultimate means of classification and unification of results, erecting the framework of intuition necessary in exploring progressively more complicated problems. To this end we consider here a novel set of shapes representing plausible equilibrium interfacial scenarios in a variety of multicomponent systems which are generating great interest in the fields of science and engineering, but lie outside the range presently accessible to accurate simulation.

We restrict attention to interfaces possessing « global uniformity », in the sense that the entire surface is completely dictated by any (arbitrarily) small piece of it. For elliptic and parabolic geometries the simplest representatives — spheres and cylinders, respectively — are specified by a single radius value alone, and accordingly, the local environment is absolutely identical throughout. The simplest representatives of the less-familiar situation of hyperbolic geometry are minimal (i.e. zero mean curvature) surfaces. Any minimal surface may be

(*) *Permanent address* : Department of Inorganic Chemistry, The Royal Institute of Technology, S-10044 Stockholm, Sweden.

expressed parametrically in the form [1]

$$(x, y, z) = \operatorname{Re} \int^{\omega} (1 - \omega'^2, i(1 + \omega'^2), 2\omega') R(\omega') d\omega', \quad (1)$$

and is thus specified solely by its particular complex analytic function $R(\omega)$. Consequently it may be generated from any region *via* analytic continuation of this so-called Weierstrass function. Note that multiplication of $R(\omega)$ by the constant $e^{i\theta}$, for real-valued θ , defines a one-parameter family of isometric minimal surfaces, referred to as the Bonnet associates of the original ($\theta = 0$) surface [2].

One would anticipate these simplest examples (determined by the least amount of mathematical input) to be favoured as equilibrium dividing surfaces in fluid partitioning problems since their construction offers the easiest routes for self-assembly. This is indeed the case for mixtures of surfactant with water and/or oil [3], and for block copolymers (with or without homopolymers) [4], in which the observed structures match these shapes (or straightforward variants of them). While the observation of spheres and cylinders (including planes as their common limiting state) conforms to our comfortable geometrical prejudices, the interpretation of the bicontinuous phases presents a greater challenge. In contrast to the spherical and cylindrical cases, the parametric representation (1) cannot, in general, guarantee that continuation gives rise to a complete surface dividing space into two distinct regions (i.e. sealing inside from outside). The global responsibilities of bicontinuity impose a selectivity, admitting only particular forms of the Weierstrass function $R(\omega)$. The ordered partitions generated by these forms are referred to as intersection-free Infinite Periodic Minimal Surfaces (IPMS). In this study we identify and parametrise a previously unknown family of such IPMS. The origin of this family is the simplest (and first discovered) IPMS, reviewed briefly in the following section.

The D , P and G minimal surfaces.

The D and P surfaces of Schwarz [5] mark the birthplace of IPMS parametrisation. The basic element of the D surface is defined by the two linear edges (AB and BC) and the planar-curve edge (AC) sketched in figure 1, subject to the boundary conditions of twofold rotational symmetry across these two straight segments and mirror reflectional symmetry over the curved segment. Repeated application of these boundary operations yields the 96 such elements comprising the fundamental unit of the D surface, i.e. the primitive unit cell of the oriented

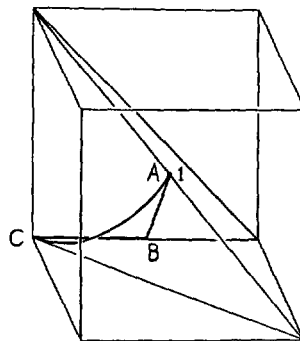


Fig. 1. — The D surface element ABC, lying within the quadrirectangular tetrahedral subdivision of the unit cube. The numeral 1 indicates that A is a first-order flat point of the surface.

surface. The topology and symmetry characterizing this fundamental unit are specified by the genus of 3 and the space group-subgroup pair $Pn\bar{3}m-Fd\bar{3}m$, respectively [6].

In equation (1) ω is the point in the complex plane stereographically projected from the Gauss map image of (x, y, z) , i.e. from the point on the unit sphere given by the direction of the vector normal to the surface there. We derive the Weierstrass function $R(\omega)$ of a given minimal surface by interpreting particular surface features *via* equation (1) as necessary properties of the requisite $R(\omega)$. As a complex analytic function is dictated by its singularity structure, we address the degeneracies of the surface — the « flat » points — at which the Gaussian curvature vanishes. The degree of a flat point (x, y, z) is the winding number of the Gauss map about this site. Its projected normal vector ω is then a branch point of the Weierstrass function, of order equal to the degree less one.

The genus of an IPMS fundamental unit is simply related to the total of its flat point degrees [7]. In particular, a genus of 3 — the lower limit of IPMS topology — corresponds to exactly eight flat points of degree two. An IPMS of genus 3 is then generated by a Weierstrass function, possessing first order branch points at the set of eight projected normal vectors $\{\omega_i\}_{i=1}^8$, of the form

$$R(\omega) = e^{i\theta} \prod_{\substack{i=1 \\ \omega_i \neq \infty}}^8 (\omega - \omega_i)^{-1/2}, \tag{2}$$

in which θ is taken, without loss of generality, to be real (modulo π), and the product is restricted to the finite images [7]. Any such surface (e.g. the D surface discussed above) thus amounts to a particular choice of $\{\omega_i\}_{i=1}^8$ and θ .

The second characteristic of an IPMS fundamental unit, its crystallographic symmetry, is interpreted in the Gauss map as orientational symmetry, describing the pattern of the distribution of flat point normal vectors on the unit sphere, or equivalently, their projected distribution in the complex ω -plane [7, 8]. The basis for classification of these patterns is the list of regular geodesic triangulations of the sphere [9]. Thus, for IPMS of genus 3, we analyse the possible patterns of a set of eight points (representing $\{\omega_i\}_{i=1}^8$) with respect to the projections of these triangular tilings.

The most symmetric option is provided by the spherical triangle with edges given by the three great circle arcs meeting at vertex angles $\pi/3, \pi/2$ and $\pi/4$. On reflection, 48 of these triangles perfectly tile the sphere, as shown in projection in figure 2. The set of eight $\pi/3$ vertices of the tiling are symmetrically equivalent under the group defined by these operations. Choosing $\{\omega_i\}_{i=1}^8$ to coincide with their positions, i.e. $\{0, \infty, \frac{1}{\sqrt{2}}, \frac{1}{\sqrt{2}} e^{i 2 \pi/3}, \frac{1}{\sqrt{2}} e^{-i 2 \pi/3}, -\sqrt{2}, \sqrt{2} e^{i \pi/3}, \sqrt{2} e^{-i \pi/3}\}$, the resulting Weierstrass functional form is given from equation (2), on expansion, by

$$R(\omega) = e^{i\theta} \left(\omega \left(\omega^6 + \frac{7}{4} \sqrt{2} \omega^3 - 1 \right) \right)^{-1/2} \tag{3}$$

In this case the entire pattern is derived by (projected) reflection of the single triangle (the region shaded in Fig. 2). On substitution of equation (3), the evaluation of equation (1) within this region of the ω -plane yields the basic element of the surface. Reflection of the triangle then defines the analytic continuation of the Weierstrass function to the adjoining region, and accordingly, the extension of the surface element *via* equation (1). Repeating this procedure, the 96 triangles comprising two identical copies of the tiling in figure 2 — spanning the

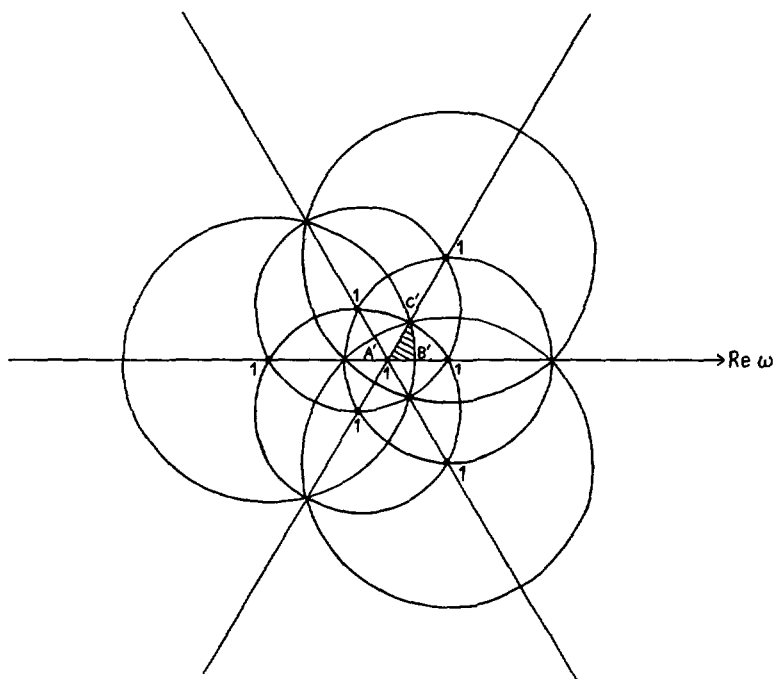


Fig. 2. — The complex ω -plane, decorated with the stereographically-projected tiling of the unit sphere generated by the $(\pi/3, \pi/2, \pi/4)$ geodesic triangle (corresponding to the shaded region A'B'C'). The eight $\pi/3$ vertex sites (implicitly including the point at infinity), affixed with the numeral 1, are the first-order branch points of the Weierstrass function in equation (3).

complete domain of single-valued definition of the dual-valued Weierstrass function in equation (3) — generate the 96 surface elements forming the fundamental unit.

As mentioned above, this approach imposes orientational order on the minimal surface, a necessary but insufficient condition to guarantee translational order giving rise to an IPMS. To ascertain this property one must further analyse the real space manifestation of the symmetries of the image space tiling [7, 8].

For the value $\theta = 0$ the triangle edge reflection continuing the Weierstrass function in equation (3) effects a pure crystallographic extension of the surface element. From equation (1) the bounding segments AB and BC of the element, with images corresponding to the triangle edges A'B' and B'C' in figure 2, must be straight lines defining axes of twofold rotation, while the third segment AC (imaged to A'C') must lie in a plane defining mirror reflection. Hence, on comparison with figure 1, the case $\theta = 0$ is precisely the Weierstrass function of the *D* surface (given in a form different, but equivalent, to the usual equation [5] due to our choice of coordinate orientation implicit in Fig. 2).

The property of pure crystallographic extension is shared by the $\theta = \pi/2$ surface, termed the « adjoint » to the $\theta = 0$ surface. However now the roles are reversed, with the triangle edges A'B' and B'C' giving rise to mirror plane curves AB and BC, and A'C' a twofold rotational line AC, bounding the surface element. This element, inscribed in the quadrirectangular tetrahedron in figure 3, is precisely that of the *P* surface. The familiar (*genus 3*) fundamental unit, constructed from the 96 such elements, possesses the symmetry $\text{Im}\bar{3}m\text{-Pm}\bar{3}m$ [6].

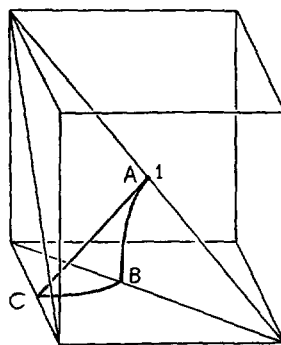


Fig. 3. — The P surface element, labelled analogously to figure 1. In both cases the projected Gauss map image of the element is the shaded triangle in figure 2 (with the prime symbols denoting the corresponding vertex images).

The crystallographic nature of the boundary conditions renders visualization of the D and P surfaces straightforward. For example, one may view the surface patch bounded by the shortest straight line circuit (obtained by mirror reflection(s) of the elements in Figs. 1 and 3) by dipping a wire frame into soap solution. Similarly it permits immediate classification of the symmetries of these two surfaces, and verification that both are free from self-intersections.

Now consider the intermediate range $0 < \theta < \pi/2$ of the Bonnet associate family generated by equation (3) (note that the surface for θ is symmetrically equivalent to its counterpart for $-\theta$ by virtue of the invariance of figure 2 under the operation $\omega \rightarrow \bar{\omega}$, i.e. reflection in the real axis $\text{Im } \omega = 0$). This range is more difficult to assess since the analytic continuation of the Weierstrass function effected by the triangle reflection does not possess a simple geometric interpretation in real space. The surface element is no longer bounded by straight lines and/or planar curves, and its extension *via* equation (1) now represents a complicated hybrid of twofold rotation and mirror reflection. The only point group symmetries retained from the original surface are the perpendicular rotational symmetries (i.e. the invariances on rotation about a surface normal, with or without inversion through the surface point) [7, 8]. Translational order can only result if the spatial distribution of these point group symmetries is globally consistent with a three-dimensional space group. It is found that imposition of a single constraint is necessary and sufficient to force this lock-in of sites, reducing the problem to the solution of one equation in the one degree of freedom θ . Schoen discovered that there exists one (and only one) value: $\theta \approx 0.66348$ ($\approx 38.015^\circ$) giving rise to an ordered surface without self-intersections, christened the gyroid [10]. The gyroid (or G , or Y^* , surface) has genus 3 and symmetry $Ia\bar{3}d-I4_132$ [6].

The D , P and G surfaces together serve as a spectacular illustration of the utility of the Weierstrass representation (1). The existence of the D and P surfaces is apparent from the initial statement of the boundary value problems defining their surface elements. The solutions of these problems, then supplying the quantitative surface details, may be derived by *ad hoc* methods based on assumptions of particular functional forms governing their implicit equations [11]. However the generality of the parametric equation (1) provides an economical unification of their descriptions *via* the simple transformation relating the two surfaces. Importantly this transformation also yields the G surface, inaccessible by any other means owing to the inseparability of its existence problem and its solution.

The family of three Bonnet-related surfaces constitute the only intersection-free IPMS of genus 3 and cubic symmetry. As such, they are the simplest bicontinuous partitions. One of the

earliest examples in their rapidly expanding range of applications involved modelling the shapes underlying « cubic phases » of lyotropic liquid crystalline assemblies [12]. Closer inspection revealed that this compositional region of the phase diagram is often sheathed by so-called « intermediate phase » regions. The available information suggests that these intermediates are likewise described by hyperbolic geometry, but of lower (typically rhombohedral or tetragonal) symmetry. In certain cases [13] the measured unit cell parameters, varying smoothly through the intermediate region, pass (nearly) continuously across the phase boundary to the cubic region, implying that the cubic structure is merely the maximal symmetry endpoint of the intermediate structural family.

To geometrically model these transitions we consider lower-symmetry IPMS families derived from cubic IPMS. In keeping with our limitation to the simplest such surfaces (D , P and G), we restrict the analysis to the simplest of their generalizations, for which the topology is preserved throughout. With the genus retaining its value of 3, the preliminary results opening this section still apply — specifically, the Weierstrass function retains the form given in equation (2). The task is thus reduced to studying the effect of symmetry reduction on $\{\omega_i\}_{i=1}^8$ and θ . The following section addresses one particular mode of degradation.

Rhombohedral generalizations.

The abovementioned nature of the bounding segments of the D and P surface elements facilitates direct derivation of their lower-symmetry variants by crystallographic deformation of a suitably chosen unit with boundary defined by symmetry operations common to both the original and degraded space groups. For rhombohedral deformations the unit is taken in both cases to be the ring-like piece (comprising 48 cubic surface elements) spanned by a pair of equilateral triangles related by $\pi/3$ screw rotation along their common axis [10, 14]. The one-variable family is then generated by stretching along this axis. Since the D and P surfaces are both special cases of this stretch, their rhombohedral generalizations are coincident (up to reorientation) and are denoted the rPD family. The surface element ABDC of a typical family member, delimited by the adjacent mirror planes slicing one-sixth of the ring-like piece, is displayed in figure 4. Note that the element possesses an internal twofold rotational symmetry perpendicular to the surface (and to the stretch axis). The rPD fundamental unit, constituting two ring-like pieces, has symmetry $R\bar{3}m-R\bar{3}m(2c)$ [6].

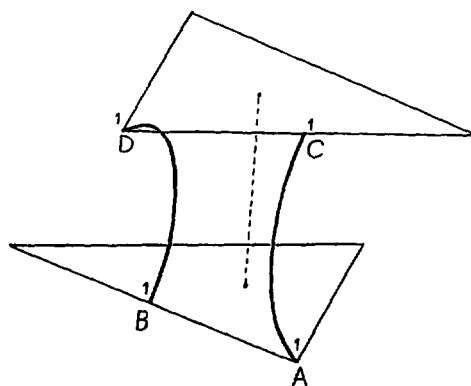


Fig. 4. — An rPD surface element ABDC. Each of its four vertices is a first-order flat point (with the pairs A and D, together with B and C, interchanged *via* the internal twofold symmetry).

In the projected Gauss map the rhombohedral deformation of the D and P surfaces corresponds to systematic degradation of the group of reflection symmetries given by the tile edges in figure 2 [8]. The six circles are removed, leaving the three straight line reflection axes ($\text{Im}(\omega^3) = 0$), together with the symmetry operations produced by composition of reflections across the pairs of these circles intersecting perpendicularly at the six sites $\omega^6 = -1$. The reduced subdivision underlies figure 5, with the open circles marking these six sites. The (generic) set of two vertices and six edge points is $\{0, \infty, t, t e^{i 2 \pi/3}, t e^{-i 2 \pi/3}, -\frac{1}{t}, \frac{1}{t} e^{i \pi/3}, \frac{1}{t} e^{-i \pi/3}\}$, where $t > 0$. Taking this one-variable pattern as $\{\omega_i\}_{i=1}^8$ (represented by the filled circles affixed with the numeral 1 in Fig. 5), substitution into equation (2), followed by expansion, gives

$$R(\omega) = e^{i\theta} \left(\omega \left(\omega^6 + \left(\frac{1}{t^3} - t^3 \right) \omega^3 - 1 \right) \right)^{-1/2} \tag{4}$$

The pattern is generated by reflection alone from the shaded region $A'B'D'C'$ in figure 5, the region of integration in equation (1) giving rise to the surface element.

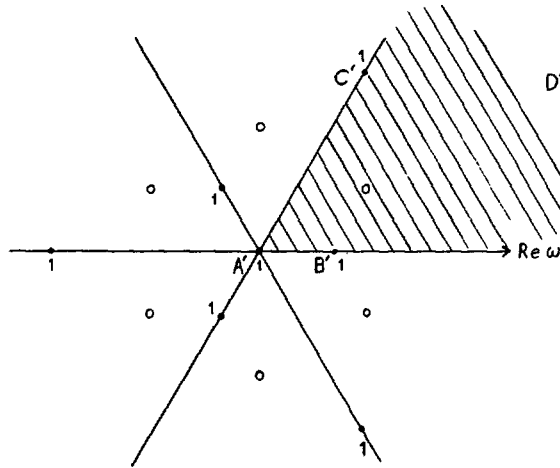


Fig. 5. — Degradation of figure 2, preserving only the straight-line reflection axes at angles $\pi/3$ and the twofold rotational symmetries at the open-circle sites. The shaded region now defines the smallest reflectional unit of the reduced tiling. The eight points labelled 1 are the symmetry images of the origin A' and the variable edge point B' ($\omega = t$), e.g. the point at infinity D' and the edge point C' ($\omega = 1/t e^{i \pi/3}$) are their respective images under the twofold operation at $\omega = e^{i \pi/6}$. These eight sites constitute the first-order branch points in equation (4).

For $\theta = 0$ (respectively $\theta = \pi/2$) the segments $A'B'$ and $D'C'$ (respectively $A'C'$ and $D'B'$) become twofold rotational lines on the element boundary, closed by the mirror plane curves from the segments $A'C'$ and $D'B'$ (respectively $A'B'$ and $D'C'$). By comparison with the discussion in the preceding section, this pair of one-parameter families defines exactly the rhombohedral deformations of the D and P surfaces, respectively, restoring the cubic IPMS as the special case $t = \frac{1}{\sqrt{2}}$. Further, combination of equations (1) and (4) verifies that the two are the same, mapping onto each other by the reorientational transformation $\omega \rightarrow \frac{1}{\omega}$ (and

$t \rightarrow \frac{1}{t}$). Hence the *rPD* family is defined continuously and uniquely *via* equation (4) by the juxtaposition of $\theta = 0$ for $0 < t \leq 1$ and $\theta = \pi/2$ for $1 \geq t > 0$, or equivalently by $\theta = 0$ only (say) for all $t > 0$ (the latter now giving the *D* and *P* surfaces at $t = \frac{1}{\sqrt{2}}$ and $t = \sqrt{2}$, respectively).

In precise analogy with the cubic case, the in-surface twofold lines and the mirror planes of these two Bonnet endpoints are non-existent in the bridging range $0 < \theta < \pi/2$ (with the surface for θ again equivalent to that for $-\theta$ since reflection symmetry in $\text{Im } \omega = 0$ is preserved in Fig. 5), necessitating a more detailed consideration of global surface properties. It is now found that the requirement of translational order imposes a pair of external constraints, i.e. a system of two coupled equations in the two free variables t and θ . However the sole solution in the range $0 < t \leq 1$, $0 < \theta < \pi/2$ which further satisfies the intersection-free criterion is $t = \frac{1}{\sqrt{2}}$, $\theta \approx 0.66348$, recovering the cubic *G* surface of Schoen.

Thus the generalization of the cubic surfaces *D* and *P* to the *rPD* family does not support a corresponding generalization of their associate surface *G*. (This corrects an earlier assertion by one of the authors [14].) The gyroid cannot be reduced in symmetry rhombohedrally by composition of this deformation of the parent *D* (or *P*) surface with Bonnet transformation, replicating Schoen's conclusion regarding orthorhombic deformations [10]. Hence this particular route cannot lead to any additional freedom.

Schoen extends his conclusion with the proposition that « there does not exist any body-centred orthorhombic version of *G*, however it is obtained », as evidence for his belief in the likelihood that « *G* may not have any variant forms of lower symmetry » [10]. Accordingly it is widely assumed in the literature that the gyroid is rigid within the class of intersection-free IPMS. Assessment of the validity of this assumption is complicated by the earlier-mentioned inseparability of existence and solution for IPMS devoid of both in-surface twofold rotation and mirror reflection operations. In the remainder of this study we resolve this open question *via* explicit construction of the family of rhombohedral variants.

The above observations regarding the Weierstrass functional form (4) indicate that the present rhombohedral deformation is an insufficiently general basis for the associate family. It is necessary to consider further generalization, corresponding to degradation of the group of symmetry operations in figure 5, admitting a symmetry reduction within its generic set of eight points. The obvious step is removal of the three straight line reflection axes, retaining however the threefold symmetry induced by composition at their two intersection sites (the origin and the point at infinity). This reduced pattern, underlying figure 6, furnishes the (generic) set of eight points $\{0, \infty, \omega_0, \omega_0 e^{i 2 \pi/3}, \omega_0 e^{-i 2 \pi/3}, \frac{-1}{\omega_0}, \frac{1}{\omega_0} e^{i \pi/3}, \frac{1}{\omega_0} e^{-i \pi/3}\}$, where ω_0 is some complex number. Identifying this two-variable set as $\{\omega_i\}_{i=1}^8$ (represented by the distribution of filled circles bearing the numeral 1 in Fig. 6), equation (2) now yields

$$R(\omega) = e^{i\theta} \left(\omega \left(\omega^6 + \left(\frac{1}{\omega_0^3} - \omega_0^3 \right) \omega^3 - 1 \right) \right)^{-1/2} \quad (5)$$

Without loss of generality we may restrict $\omega_0 = t e^{i\phi}$ to lie in the region defined by $t = |\omega_0| > 0$, $-\pi/6 < \phi = \arg \omega_0 \leq \frac{\pi}{6}$. For an arbitrary such value, the smallest symmetry unit (taken, for example, as this region $|\arg \omega| \leq \frac{\pi}{6}$ shaded in Fig. 6) is no longer delimited

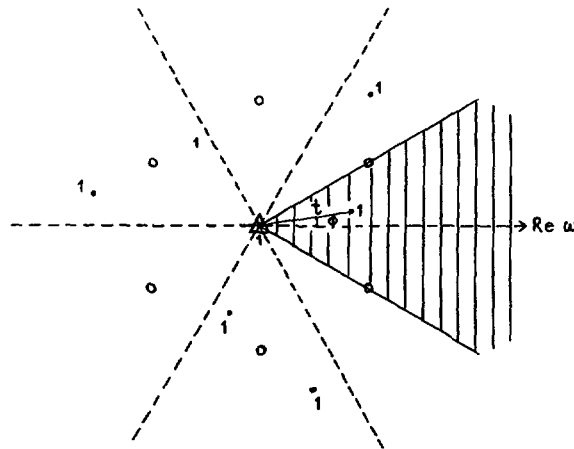


Fig. 6. — Degradation of figure 5, replacing the reflection axes by threefold symmetry sites (triangle symbol) at the origin and at infinity. The shaded region represents a basic unit of the scheme, and contains the point $\omega_0 = t e^{i\phi}$. The rotational operations give rise to the set of six related points which, together with the threefold sites, define the eight branch points (marked 1) of the Weierstrass function in equation (5).

by edges of reflection — it now generates the entire pattern via the twofold (open circle symbol)- and threefold (triangle symbol)- composite operations alone. Consequently the basic surface element, obtained by integration of equation (5) in the representation (1) over this region, cannot be extended by a « boundary segment-fixing » crystallographic mechanism for any θ value. Instead the element is swivelled around its boundary by the perpendicular rotational symmetries 2 and 3 effected by these composite operations, for all θ .

Note that the Weierstrass function in equation (5) embraces all previously known examples of genus 3, intersection-free IPMS with (at least) trigonal symmetry. Clearly it degenerates into the two-variable form (4) for the special case $\phi = 0$. At the other extreme, the limit $\phi = \pi/6$ gives the two-variable family

$$R(\omega) = e^{i\theta} \left(\omega \left(\omega^6 - i \left(\frac{1}{t^3} + t^3 \right) \omega^3 - 1 \right) \right)^{-1/2}, \tag{6}$$

which likewise restores reflection axes in figure 6, now delimiting the region $|\arg \omega| \leq \frac{\pi}{6}$, $|\omega| \leq 1$ as the smallest symmetry unit. For this orientation the values $\theta = \mp \frac{\pi}{4}$ correspond to the pair of cases for which these reflection axes are realised as twofold rotational lines and mirror plane curves bounding the surface element. Specifically, $\theta = \frac{-\pi}{4}$ defines the one-variable family of H surfaces discovered by Schwarz [5], while the $\theta = \frac{\pi}{4}$ (adjoint H) surfaces are (crystallographically) self-intersecting. The bridging range $\frac{-\pi}{4} < \theta < \frac{\pi}{4}$ (with the surface for θ now symmetrically equivalent to that for $\pi/2 - \theta$ by virtue of the symmetry $\omega \rightarrow e^{i\pi/3} \bar{\omega}$, i.e. the reflection axis $\text{Im}(e^{-i\pi/6} \omega) = 0$) was investigated in a previous study by one of the authors [15]. The two conditions in t and θ necessary for translational order were found to yield an intersection-free IPMS for the solutions $t \approx 0.5361$ and $\theta \approx 0.3353$ ($\approx 19.21^\circ$). This IPMS, denoted here the HG surface, possesses fundamental unit of symmetry

R3c-R32 [16]. Significantly, it represents a simple counterexample to Schoen's claim, regarding his G surface, that « it is considered highly unlikely that any other intersection-free IPMS containing neither straight lines nor plane lines of curvature will be found » [10].

While the G and HG surfaces are unique within the Bonnet associates of the one-variable rPD and H surface families, respectively, equation (5) supplies the extra degree of freedom, ϕ , necessary to relax their rigidity. The original states $((t, \phi) = \left(\frac{1}{\sqrt{2}}, 0\right)$ and $(t, \phi) \approx \left(0.5361, \frac{\pi}{6}\right)$, respectively) may now be perturbed two-dimensionally throughout their generic neighbourhood in the complex ω_0 -plane. This will open up a one-dimensional continuum of solutions (corresponding to intersection-free IPMS) emanating from the two sources. Further, the unifying nature of equation (5) dictates that these two solution curves may be smoothly continued into each other. This single curve will then be the required one-variable generalization connecting the previously isolated G and HG surfaces. By establishing the link, this new family, denoted rG , thus provides the simplest path of continuous, zero mean curvature-preserving access between the rPD and H families. The stretched rPD family is relaxed to restore the cubic special case (either D or P), which is first bent (*via* the Bonnet transform) into G , distorted into HG , and then bent back to the H surface to regain its generic degree of stretching freedom.

The quantitative features of the numerically generated rG family are presented in the following section.

Results.

The one-variable rG family is defined by the two equations in the set of three variables, ϕ, t, θ imposing translational order. The family is conveniently indexed by ϕ such that, for a particular member i.e. ϕ value, the system is solved for the corresponding t and θ values fixing the branch point position and the Bonnet angle. The pair of equations, obtained *via* substitution of equation (5) into the representation (1), enforce the lock-in of parallel threefold axis sites. As they are identical to the constraints applied previously to the HG surface [15], the solution procedure is not detailed here. It is computationally well-behaved since the coupling between the two variables t and θ is only slight.

Note that the absence of edges of reflection symmetry in figure 6 (in particular, the axis $\text{Im } \omega = 0$ for the rPD family and $\text{Im}(e^{-i\pi/6} \omega) = 0$ for the H family) removes any symmetrical degeneracies within the full range of θ (modulo π). Thus, in the interval $0 \leq \phi \leq \pi/6$ there exist distinct pairs of solution families diverging in $\phi \geq 0$ from the two symmetrically equivalent $\phi = 0$ values ($\theta \approx 0.66348$ and $\theta \approx -0.66348$) for the G surface and similarly in $\phi \leq \pi/6$ from the $\phi = \pi/6$ alternatives ($\theta \approx 0.3353$ and $\theta \approx \frac{\pi}{2} - 0.3353$) for the HG surface. It is found that the families corresponding to the first-mentioned θ option in these two cases merge continuously into the connecting solution. The solution thus derived, i.e. the polar coordinate curve $t = t(\phi)$ and the association parameter curve $\theta = \theta(\phi)$ for $0 \leq \phi \leq \pi/6$, is plotted in figure 7.

The simple nature of the trends in these variables is likewise manifested in the appearance of the rG surface family itself. In figure 8 the scan of the range displays surface pieces of this solution family for three different ϕ values. In each case the pieces are generated from identical regions of the complex ω -plane and are viewed down the common threefold axis direction. The intermediate member $\phi = \pi/9$ in figure 8b confirms the monotonic transition reducing the tunnels in this direction from their largest width in the G surface case $\phi = 0$ (Fig. 8a) to their smallest at the HG case $\phi = \pi/6$ (Fig. 8c).

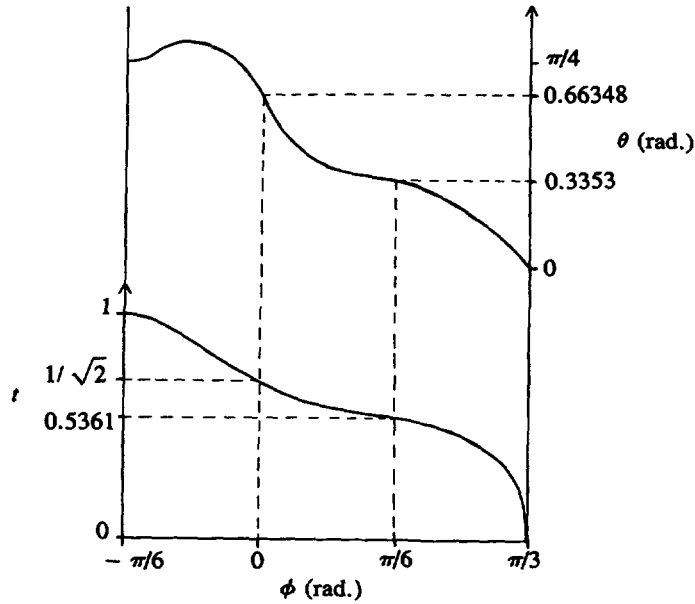
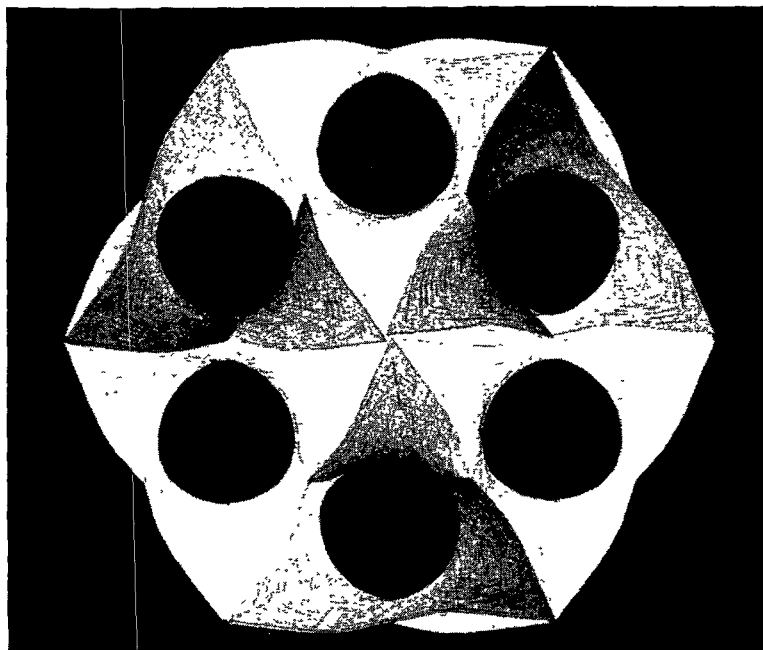


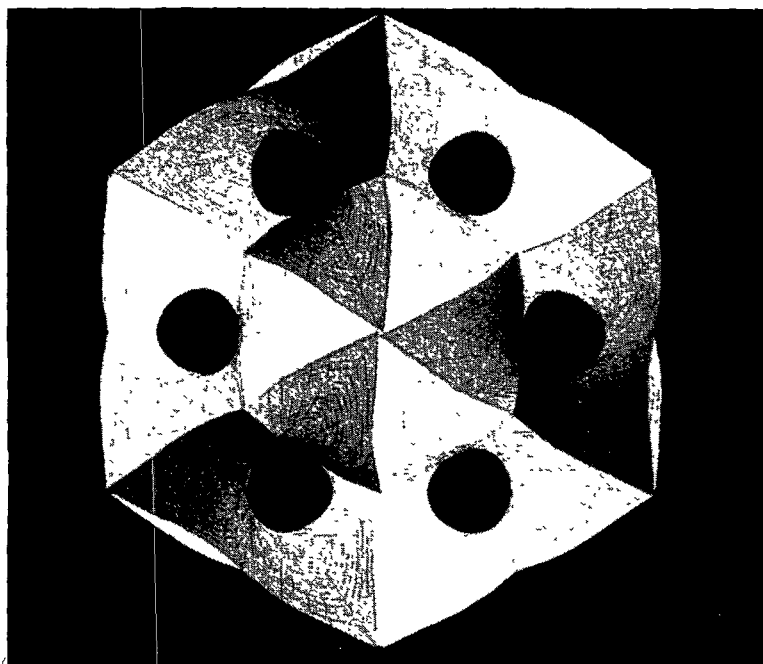
Fig. 7. — The solution defining the entire family of rG surfaces in terms of the single parameter ϕ . The corresponding radial ordinate t (left axis) and Bonnet angle (right axis) are plotted for each ϕ . The special values $\phi = 0$ and $\phi = \pi/6$ represent the known cases of the G and HG surfaces, respectively.

Further, recall that there also exist solution families emanating from the two special cases $\phi = 0$ and $\phi = \pi/6$ corresponding to their second-mentioned θ options above. These two extra families, on reflection in their bounding axes (i.e. in $\text{Im } \omega = 0$ so $\omega \rightarrow \bar{\omega}$ and $\phi \rightarrow -\phi$, taking θ to $-\theta$, and in $\text{Im}(e^{-i\pi/6} \omega) = 0$ so $\omega \rightarrow e^{i\pi/3} \bar{\omega}$ and $\phi \rightarrow \pi/3 - \phi$, taking θ to $\pi/2 - \theta$, respectively) are smooth continuations of the connecting solution in $0 \leq \phi \leq \frac{\pi}{6}$ (given by the first-mentioned values) to the ranges $\phi \leq 0$ and $\phi \geq \pi/6$, respectively. The associated solution curves $t = t(\phi)$ and $\theta = \theta(\phi)$ in these supporting ranges are likewise graphed in figure 7. The existence of these extensions is apparent from extrapolation of the trend illustrated in figure 8. The $\phi \leq 0$ family, for which the threefold tunnels continue to increase in size beyond the G surface value (Fig. 8a), terminates asymptotically with the case $\phi = -\pi/6$, $\theta = \pi/4$ (symmetrically equivalent to $\phi = \pi/6$, $\theta = -\pi/4$), corresponding to the H surface, in the limit $t = 1$ of infinitely-wide tunnels (so the periodic surface becomes a single saddle tower). Similarly the $\phi \geq \pi/6$ family, representing a decrease in tunnel width below that of the HG surface (Fig. 8c), ends by approaching $\phi = \pi/3$, $\theta = 0$ (symmetrically equivalent to $\phi = 0$, $\theta = \pi/2$), i.e. the rPD surface, in its vanishing limit $t = 0$.

Taken together, the continuous solution spanning the full range $-\frac{\pi}{6} \leq \phi \leq \frac{\pi}{3}$ in figure 7 defines the entire rG surface family. The symmetry of the (fundamental unit of the) generic rG surface, classifying the degradation of the cubic G surface, is precisely that of the HG case quoted above, namely space group-subgroup $R\bar{3}c$ -R32. The dependence of the ratio c/a of the rhombohedral cell dimensions, together with the surface-to-volume ratio S^3/V^2 , on the parameter ϕ may be readily extracted from the information in figure 7.

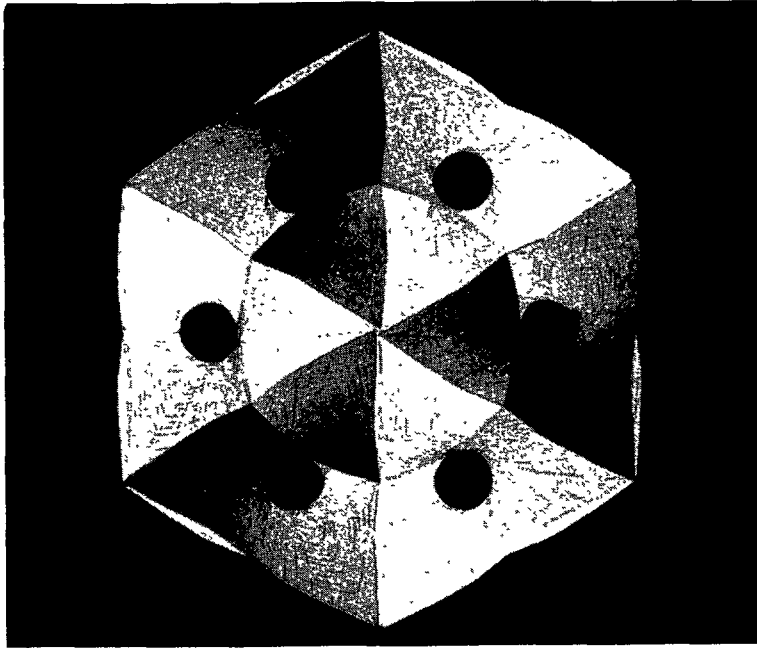


a)



b)

Fig. 8. — Computer-generated views of the same piece of the rG surface at (a) $\phi = 0$ (the G surface), (b) $\phi = \pi/9$ and (c) $\phi = \pi/6$ (the HG surface).



c)

Fig. 8 (continued).

Extensions and conclusions.

Although the preceding sections focussed on rhombohedral variants of Schoen’s gyroid, the underlying principles are not limited to this specific distortion. More generally there exists lower symmetry derivatives of the surface corresponding to systematic degradation of the tiling pattern projected in figure 2 which preserve (at most) rotational symmetries only and admit of a generic order-eight set.

Performing a coordinate reorientation, the original tiling is equally well represented in projection in figure 9. With the $\pi/3$ vertices now residing at the eight positions $\left\{ \left(\frac{\sqrt{3} \pm 1}{\sqrt{2}} \right), i \left(\frac{\sqrt{3} \pm 1}{\sqrt{2}} \right), - \left(\frac{\sqrt{3} \pm 1}{\sqrt{2}} \right), -i \left(\frac{\sqrt{3} \pm 1}{\sqrt{2}} \right) \right\}$, substitution into equation (2) yields

$$R(\omega) = e^{i\theta} (\omega^8 - 14 \omega^4 + 1)^{-1/2} \tag{7}$$

While this more familiar form [5] is precisely equivalent to that in equation (3) on application of the same coordinate transformation to the representation (1), it now facilitates a tetragonal mode of distortion. Retaining fourfold symmetry at the origin and the point at infinity i.e. $\omega = 0, \infty$ and twofold symmetry at the eight sites $\omega^8 = 1$ on the unit circle, the generalised group $\left\{ \omega_0, i \omega_0, -\omega_0, -i \omega_0, \frac{1}{\omega_0}, \frac{i}{\omega_0}, \frac{-1}{\omega_0}, \frac{-i}{\omega_0} \right\}$ then gives

$$R(\omega) = e^{i\theta} \left(\omega^8 - \left(\frac{1}{\omega_0^4} + \omega_0^4 \right) \omega^4 + 1 \right)^{-1/2} \tag{8}$$

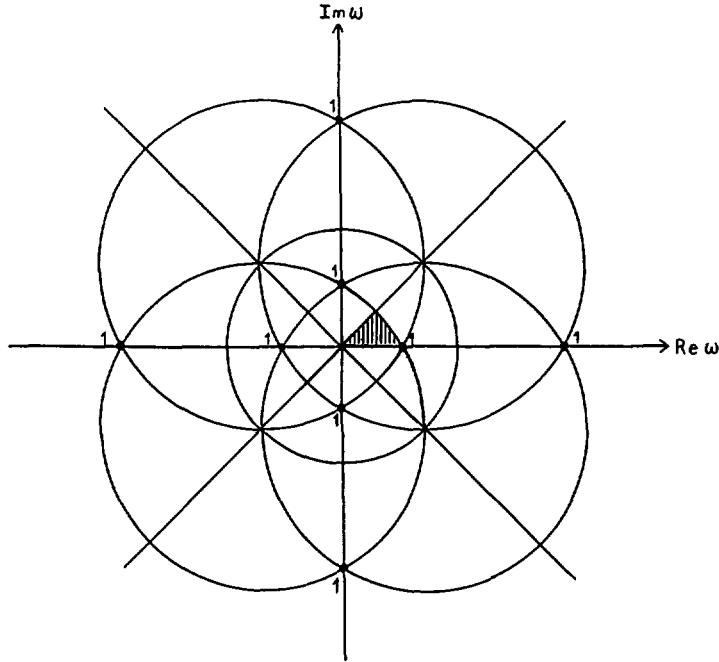


Fig. 9. — The projected tiling of the complex plane in figure 2, after a rotation mapping the $\pi/4$ vertex of the basic triangle (shaded) to the origin and the $\pi/4-\pi/3$ edge along the real axis. The new positions of the eight $\pi/3$ vertices are now the first-order branch points of the function in equation (7).

Here the complex number $\omega_0 = t e^{i\phi}$ may be assumed to lie within the region $t > 0$, $0 \leq \phi < \frac{\pi}{4}$. The special case $\phi = 0$, reinstating the reflection axes $\text{Im}(\omega^4) = 0$ and $|\omega| = 1$, defines the Bonnet associates of the one-variable family, denoted tD , of tetragonally distorted D surfaces [8]. As with the rhombohedral rPD case, the pair of equations in t , θ return the cubic gyroid $\left(t = \frac{\sqrt{3}-1}{\sqrt{2}}, \theta \approx 0.66348 \right)$ as the only intersection-free IPMS within the

range $0 < \theta < \pi/2$ bridging the tD and tP surfaces. However the presence of the additional parameter ϕ in equation (8) liberates a one-variable family of non-trivial solutions from this source point. These constitute the tetragonal variants tG of the gyroid.

The results of this study, revealing the robust nature of the gyroid, hopefully serve to demystify this surface. They illustrate that lower-symmetry variants of the gyroid follow from degradation of the spherical tiling pattern in a manner precisely analogous to that previously established for its « conventional » associates, the D and P surfaces [8].

This observation applies to all IPMS, independent of the intersection-free condition. If the $\theta = 0$ (and hence $\theta = \pi/2$) IPMS possesses an intermediate ($0 < \theta < \pi/2$) Bonnet associate which is likewise translationally ordered (but lacking in-surface, twofold rotation and mirror reflection symmetries) then both exhibit the same range of order-preserving, deformation freedom. The D surface only appears special in the sense that this intermediate member is also free from self-intersections. It is of interest to determine whether any of the (higher genus) cubic IPMS share this property. A previous investigation returned a negative answer regarding the I-WP surface of genus 4 [17]. We have subsequently analysed the simplest two members [18, 19] remaining in the known set [6, 10] of cubic IPMS — the F-RD and $C(P)$ surfaces (of

genus 6 and 9, respectively). Again no intersection-free associates were revealed. It is tempting to generalise this trend, since it appears unlikely that a topologically-complicated IPMS may be bent to the required extent without being forced to pass through itself.

Acknowledgement.

One of the authors (A. F.) was supported by the Swedish Natural Research Council (NFR).

References

- [1] Weierstrass K., Untersuchungen über die Flächen, deren mittlere Krümmung überall gleich Null ist, *Monatsber. d. Berliner Akad.* (1866) 612-625.
- [2] Bonnet O., Note sur la Théorie Générale des Surfaces, *C. R. Acad. Sci. Paris* **37** (1853) 529-532.
- [3] Fontell K., *Colloid Polym. Sci.* **268** (1990) 264-285.
- [4] Thomas E. L., Anderson D. M., Henkee C. S., Hoffman D., *Nature* **334** (1988) 598-601.
- [5] Schwarz H. A., *Gesammelte Mathematische Abhandlungen*, Vol. **1** (Springer, Berlin, 1890).
- [6] Koch E., Fischer W., *Acta Cryst. A* **46** (1990) 33-40.
- [7] Fogden A., Hyde S. T., *Acta Cryst. A* **48** (1992) 442-451.
- [8] Fogden A., Hyde S. T., *Acta Cryst. A* **48** (1992) 575-591.
- [9] Erdélyi A., Magnus W., Oberhettinger F., Tricomi F. G., *Higher Transcendental Functions*, Bateman Manuscript Project (New York, McGraw-Hill, 1953) pp. 96-99.
- [10] Schoen A. H., Infinite Periodic Minimal Surfaces without Self-Intersections, *NASA Techn. Rep. D-5541* (1970).
- [11] Nitsche J. C. C., *Lectures on Minimal Surfaces*, Vol. **1** (Cambridge University Press, Cambridge, 1989).
- [12] Scriven L. E., *Nature* **263** (1976) 123.
- [13] Kékicheff P., *Mol. Cryst. Liq. Cryst.* **198** (1991) 131-144.
- [14] Lidin S., *J. Phys. France* **49** (1988) 421-427.
- [15] Lidin S., Larsson S., *J. Chem. Soc. Faraday Trans.* **86** (1990) 769-775.
- [16] Fischer W., Koch E., private communication.
- [17] Lidin S., Hyde S. T., Ninham B. W., *J. Phys. France* **51** (1990) 801-813.
- [18] Fogden A., *J. Phys. I France* **2** (1992), 233-239.
- [19] Fogden A., *Acta Cryst. A* (in press, 1993).